Spaceborne Applications of P-band Imaging Radars for Measuring Forest Biomass

Eric J. Rignot, Reiner Zimmermann, Jakob J. van Zyl and Ram Oren

Jet Propulsion Laboratory, California Institute of Technology, Pasadena CA 91109

Ph (818) 354-1640; Fax (818) 393-6943

Abstract

In three test sites of boreal and temperate forests, P-band polarimetric radar data estimate total above ground dry woody biomass within 10 to 30% of the actual biomass values, depending on the complexity of the forest. Estimates obtained using cross-polarized data only are 1 to 11% less accurate. Over flooded forests, wet or damaged trees, and sparse open tall forests, circular-polarized radar data do not provide reliable estimates of forest biomass, because of large polarimetric phase differences. Circular polarization, which could help minimize the limiting effect of Faraday rotation in spaceborne applications, may therefore be of limited use for estimating forest biomass. In the tropical rain forests of Manu, in Peru, where forest biomass ranges from 4 kg/m^2 in young forest succession up to 100 kg/m^2 in old, undisturbed floodplain stands, P-band polarimetric data separate major vegetation formations and also perform better than expected in estimating woody biomass. The worldwide need for large scale, updated biomass estimates, achieved with a uniformly applied method, justifies a more in-depth exploration of long wavelength imaging radar applications for tropical forests inventories.

Submitted to IEEE Transactions on Geoscience and Remote Sensing

IGARSS'1994 Special Issue

December 9, 1994

1. Introduction

Several experimental studies demonstrated that radar backscatter at the longer wavelengths is positively correlated with total above ground dry woody biomass, up to a biomass level of about 20 kg/m^2 at P-band frequency ($\lambda = 68$ cm), where radar backscatter saturates [1-4]. HH (horizontally received and transmitted) and HV-polarization (horizontally received, vertically transmitted) provide a greater sensitivity to woody biomass than VV polarization. Modeling studies [5-8] suggest that P-band HV polarized radar signals originate from volume scattering interactions with the larger and lower branches of the forest canopy and are therefore strongly correlated with branch biomass. At HH polarization, contributions to total radar backscatter from the trunk-ground scattering term eventually exceed contributions from branch scattering. HH polarized signals are therefore more better correlated with stem biomass, itself a major fraction of total woody biomass [9-11]. At VV-polarization, the radar returns from trunk-ground interactions are more attenuated by the tree trunks. As a result, VV-polarized radar backscatter increases less rapidly with increasing biomass than HH-polarized radar backscatter. With a sensitivity of radars to biomass levels up to 20 kg/m^2, it is possible to map above ground biomass over grassland, shrubland and woodland [12-14], boreal forests [15], and a significant portion of temperate forests [16]. Over the world's forests, a P-band radar could contribute information for improving current estimates of the global carbon balance by mapping stored above ground biomass, and identify and quantify deforestation and forest regrowth.

For spaceborne applications of P-band imaging radars, the phenomena of Faraday rotation adds another difficulty. When a plane wave travels through the ionosphere, it splits into two circularly polarized waves having opposite senses of rotation and different phase velocities. As a result, the wave that returns from its round-trip journey through the ionosphere has a plane of polarization that has been rotated relative to its original position. The amount of rotation depends on the electron density profile in the ionosphere, the earth's magnetic field, and the square of the radar frequency [17]. The maximum likely value for Faraday rotation at P band (400 MHz) is 675° during the day and 67° at night. At L band (1.25 GHz), the predicted maximum effect is 69° rotation during the day and 7° at night. The resulting phase and amplitude errors not only affect the estimation of forest biomass from the radar data but the processing of the SAR data as well.

In April 1994 and October 1994, the SIR-C/X-SAR radar instrument onboard the space shuttle Endeavour gathered the first polarimetric, spaceborne radar images of the earth at both C and L band. During the two experiments, the calibration team reported cross talk values between H and V polarization consistently below 30 dB at L band, day and night [18]. As one would expect a significant amount of cross talk between the H-polarized and the V-polarized channels in the presence of Faraday rotation, these preliminary results suggests that Faraday rotation is negligible at L band at 200 km altitude. The situation would be different for a radar orbiting at 800 km altitude as the ionospheric electron density at sun spot maximum peaks at about 400 km altitude [17]. One technique, currently used by Global Positioning System satellites, is to transmit at two frequencies (1.575 GHz and 1.228 GHz) and combine the measurements to estimate ionospheric propagation. Since Faraday rotation at P band at night should be similar to Faraday rotation at L band during the day, similar correction techniques could probably be developed for operating a P-band radar at linear polarization at night.

One alternative solution is to operate the radar system at circular polarization as circular-polarized radar signals are less sensitive to Faraday rotation. To test that approach, we compared predicted biomass values from the radar at both linear and circular polarizations using the polarimetric radar data gathered by the NASA/JPL AIRSAR instrument over several forest sites where estimates of forest biomass have been obtained. Three examples are considered from both temperate and boreal forests. We also compare biomass estimates utilizing HV-polarized backscatter to those utilizing several polarizations to determine the added value of polarimetric information for measuring forest biomass. Finally, we examine the potential of P-band polarimetric radars to characterize the distribution in forest types and in above ground biomass of tropical rain forests. Pristine tropical forests are a large pool of stored carbon and play an important role in the short term global carbon cycle [ ]. They are a challenge to remote sensing studies because of both the high variation in biomass [3] under often uniform, closed canopies with high leaf area indices [20] and the lack of ground truth information due to their aerial extent and difficult accessibility in many regions. Here, we studied the retrieval of above ground biomass in the tropical rain forest of the Manu National Park, in Peru, which was imaged by the NASA/JPL AIRSAR instrument in June 1993. The radar results are compared to estimates of above ground biomass obtained from sample plots placed in several forest types and successional stages.

2. Airborne data and ground truth estimates

The four examples of forest considered in this study cover a wide range of forested areas: maritime pine plantations of the Landes forest, south of Bordeaux, in southwestern France (44.6 degrees North, .0 degree West) [ ]; lolloby pine plantations of the Duke University Forest, west of Durham, in North Carolina (36.0 degrees North, 79.0 West) [2]; natural boreal forests of the Bonanza Creek experimental forest, west of Fairbanks, in Alaska (64.4 degrees North, 148.2 degrees West [4]; and primary tropical rain forests of the Manu National Park, department of Madre de Dios, in south-east Peru (2.0 degrees South, 70.8 degrees West) [21-24].

The Landes forest is the largest plantation forest in France, selected as a prototype of a managed forest ecosystem. Forest stands contain even-aged maritime pine (*Pinus pinaster* Ait. Pinaceae) regularly planted in rows [ ]. A total of 30 stands have been sampled in that forest, with total above ground biomass ranging from kg/m^2 for the youngest forest stands, up to 5 kg/m^2 for 46 year-old forest stands. The area also includes many clear-cuts.

The Duke University Forest contains even aged stands of irregularly spaced lolloby pine trees (*Pinus taeda* (L.) Pinaceae) regrowing on abandoned agricultural fields. There are also many stands that contain a mixture distribution of deciduous and coniferous species. More than 100 stands have been sampled in that area with ages ranging from 2 to > 00 years, and above ground biomass ranging from 0.1 to 49 kg/m^2 [2 3]. Since some of these stands are relatively small in size in the AIRSAR images, we limited the present analysis to 11 stands with the same above range in biomass containing enough image pixels to obtain reliable measures of the statistics of the SAR signal. Both the Landes and Duke forests lay on relatively flat terrain. The forest biomass values obtained from forest inventory and allometric equations are not known with better than 10% accurac[3].

The Bonanza Creek experimental forest, BCEF, near Fairbanks, Alaska, is a LTER (Long Term Ecological Research) site representative of the boreal forests of interior Alaska. BCEF is a natural, undisturbed, boreal forest, which includes several deciduous and evergreen tree species in both floodplain and upland forests. Upland forest types on well drained, nutrient rich, and south facing slopes with no permafrost present include stands of highly productive aspen (*Populus tremuloides* (Michx.) (Pinaceae)), paper birch (*Betula papyrifera* (Marsh) (Betulaceae)) and white spruce (*Picea glauca* (Moench) Voss (Pinaceae)). On north facing slopes and poorly drained areas, black spruce (*Picea mariana* (Mill.) (Pinaceae)) forests dominate on permafrost soils with low nutrient availability. Floodplain forests contain productive stands of balsam poplar (*Populus balsamifera* (L.)) and white spruce forming on river alluvium and permafrost-free soils. Young successional stages are dominated by alder (*Alnus crispa* (Ait.) Pursh) and willow shrubs (*Salix spp.*). Older, poorly drained terraces are underlain by permafrost and contain sphagnum bogs and tamarack (Larix laricinoides) mixed with slow growing black spruce. Total above ground biomass ranges from 0.4 to 22 kg/m^2 in the 21 forest stands that were inventoried [4]. Forest biomass varies significantly within each stand. The standard deviation in forest biomass from one plot to the next is 34% of the mean stand biomass on average. Allometric equations are also not very accurate. As a results, the accuracy of our forest biomass estimates probably is not better than 20%.

The Manu National Park, Peru, is located at the remote western edge of the Amazon basin. It contains pristine, tropical rain forest types with a striking diversity of tropical tree species.

The generally humid climate is interrupted by a dry season in July August. Floodplain succession and climax forests occur on nutrient rich alluvial soils along the Rio Manu, and mature forests on more dry and leached soils on the adjacent hills. Since a biomass inventory was not available for any forest in this area, a ground team characterized the major forest types and approximate spatial distribution of vegetation along the accessible areas of the lower Manu river in September 1993. Seventeen 10 m radius plots with representative vegetation types were measured for average tree and canopy height, canopy closure, tree density and understory composition. The above-ground biomass for all forest types was estimated by applying allometric equations [9] derived from pristine South Asian forests [25]. Estimation of individual tree height from measured diameter breast height resulted in a slight underestimation of actual tree dimensions. For *Cecropia membranacea* (Moracae) stands, few estimates of forest volume were available from previous studies in the lower Madre de Dios area [24] and Panama [26] and their results are consistent with our estimations. Reported forest volumes were converted to woody biomass by using a wood density of 0.5 to account for the relative light wood of this species compared to the reported average value of 0.62 or 0.69 for tropical woods [11]. Aboveground dry biomass of early forest succession like mature *Tessaria integrifolia* (Asteraceae) and *Gynerium sagittatum* (Poaceae) 10 m in height was estimated to be 4 kg/m^2. In *Gynerium Cecropia membranacea* forest, 17 m in height, woody biomass is 4.3 kg/m^2. On abandoned high river channels with an annually varying water table, palm swamps (Aguajales) may develop. The dominating species in the open canopy is the palm *Mauritia flexuosa syn. reflexa* which reaches 25 30 m height. The understory varies widely from open sand spots with xerophytic shrubs to permanently flooded areas with dense understory (3-5 m) of banana-like *Heliconia episcopalis* (Musaceae) spec. Above ground biomass in a permanently inundated Aguajal (max. 22 m height) was estimated to be 13 kg/m^2, 17 kg/m^2 in a mainly dry and open Aguajal (26 m), and 8 kg/m^2 in a typical Aguajal (28 m) with moist soil and a high palm density. Broadleaf fores types along the Rio Manu are evergreen to semi-deciduous with wide variations in canopy st11('(111". In the floodplain, we calculated for a mosaic forest (>27 m) on rich alluvial soil a biomass of 31 kg/m^2. On adjacent hills, forests vary from tall stands with closed canopies to open semi-deciduous stands. We calculated 28 kg/m^2 for a semi deciduous upland forest (30 m) and 46 kg/m^2 for a tall forest (40 m) with ('1(1)('(1 overstory. For these two stands the estimated leaf area index ((i.I) \ \'ir; very similar, and the apparent large difference of below canopy biomass may be a result of different water and nutrient availability for tree growth. Total above ground biomass of a tall (>50 m), old grown floodplain forest at Cocha Cashu, Rio Manu, was estimated to be 104 kg/m^2. This value probably represents the highest above ground biomass accumulation found in this area due to the large size of individual trees reaching emergent tree heights of 53 m, with diameter at breast height (dbh) of 3 m, and a closed canopy of dominant trees with dbh between 0.9 and 2.4 m [27]. The estimated biomass values for mature old grown floodplain clearly ('X("('(I the report 1 ('(1 average value of 67 ii{\/J11' for high dense tropical forests of the generally poor soils on Terra l'1II [1(' in the Brazilian forests [11]. However, in general, even higher forest volumes are possible and have been repeatedly reported for temperate coastal rain forests in higher latitudes [? Since the impressive mature floodplain forests cover relatively small areas, the average above ground biomass weighed by the area covered by each species is however expected to be 111(1("11 lower. Reported average potential biomass values for forest areas without human impact in tropical Asia are 45-54 kg/m^2 for moist lowland, 35-45 kg/m^2 for lowland seasonal and 24 kg/m^2 for dry seasonal types [29].

3. Predicted versus actual biomass in temperate and boreal forests

In the forest sites from Alaska, Duke and Landes, we extracted the radar response of 11(" forest from polygonal areas where ground truth information had been ('(111 ('('(('(1 [I-I]. Radar backscatter was [11(')1 plotted as a function of biomass and regression curves were derived to predict biomass from the radar. The regression curves are second order polynomials in radar backscatter, relating the natural logarithm of the biomass, $Log(B)$, to σ^o_{HV} in dB, or to a vector containing σ^o_{HV}, σ^o_{HH} and σ^o_{VV}, all expressed in dB. Similar regressions were derived to relate biomass to σ^o_{RR} (right-circular received and transmitted), or to a vector containing σ^o_{RL} (right-circular received and left-circular transmitted) and σ^o_{RR}. Predicted biomass levels from the radar data were then compared to actual biomass levels. An error was computed as the average absolute difference between predicted and actual biomass, expressed in percent of actual biomass. This error measures the degree of spread between the points used in the regression analysis and the points obtained from a best fit of the data (Table I). We find this measure more representative of the degree of confidence that can be placed in the radar estimates of biomass than, for instance, the coefficient of determination, r^2, which is usually greater than 90 % (Table I).

For the Landes forest, the average absolute error in biomass is about 11% at both linear and circular polarization. Results obtained with HH-, HV, and VV-polarization combined are only slightly better than those obtained using HV-polarization alone.

For the Duke University Forest, the error rates are higher than those obtained for the Landes forest. This result was expected because the stands are less homogeneous, not always dominated by a single tree species, and of much higher biomass. Linear and circular polarizations yield similar predicted biomass levels, except for two stands of low biomass where circular-polarized signals overestimate the woody biomass. In those two stands, the polarimetric phase difference (or phase difference between HH- and VV polarization) is 31° greater than that recorded in neighboring stands of similar biomass, and σ^o_{RR} is several dB larger. We believe these two stands are more open and more sparse than the neighboring stands. As we shall see later on, this situation favors trunk-ground scattering interactions, which yield large polarimetric phase differences, increase σ^o_{RR} and yield to an overestimation of forest biomass.

For BCEF, error rates for the July 1993 data are about 20 to 30 % of the actual values, again higher than that for the Landes forest. It was expected that in natural forests the retrieval of forest biomass would be more difficult because the spatial variability in tree height, age, density, diameter and species is more pronounced within each stand. Using several polarizations together, instead of independently, improves the results significantly. We subsequently examined the stands with the largest errors at circular polarization. The biomass level of alder stands in 1993 is always overestimated, even at linear polarizations. However these alder stands had been severely damaged in 1992 and all trees were either broken or lying on the ground. In two mixed stands of white spruce and balsam poplar trees, forest biomass was also overestimated at circular polarization. These two stands were characterized by a polarimetric phase difference of about 70 to 94^o at P-band, significantly larger than that observed in other forest stands of similar biomass. We visited one of these stands in 1991 and found that balsam poplar trees were rotten, with very wet tree trunks. Strong double bounce interactions between the soaked tree trunks and the ground layers probably explain the large polarimetric phase differences recorded in those stands.

The error in predicted biomass is very large at circular polarization on May 3, 1991, when the floodplain forests were flooded (Table 1). The error is lower on May 6, once the forest is no longer flooded. Between May 3, 1991 and July 21, 1993, the polarimetric phase difference of mature white spruce and balsam poplar stands in the floodplains decreased from about 100^o on average to an average of about 54^o. As we shall see next, large polarimetric phase differences caused by enhanced trunk-ground scattering, yield large values of the radar backscatter in RR-polarization, which generally results in an overestimation of forest biomass.

For azimuthally symmetric, natural, distributed targets, which is the case of most forests, we may assume that the components of the scattering matrix S_{HH} and S_{HV} as well as S_{VV} and S_{HV} are uncorrelated, and $S_{HV} = S_{VH}$ [30]. The average cross products at circular polarization are then simplified as

$$< S_{RL}S_{RL}^* > = \frac{< S_{HH}S_{HH}^* >}{4} + \frac{< S_{VV}S_{VV}^* >}{4} + 0.5Re(< S_{HH}S_{VV}^* >) \quad (1)$$

$$< S_{RR}S_{RR}^* > = \frac{< S_{HH}S_{HH}^* >}{4} + \frac{< S_{VV}S_{VV}^* >}{4} + < S_{HV}S_{HV}^* > - 0.5Re(< S_{HH}S_{VV}^* >) \quad (2)$$

If $\phi_{HHVV}^* \approx 180^o$ and S_{HH} and S_{VV} are highly correlated and nearly equal in magnitude, we have $< S_{RL}S^*_{RL} > \approx 0$, and $< S_{RR}S^*_{RR} > \approx < S_{HH}S^*_{HH} > + < S_{HV}S^*_{HV} >$. With S_{HH} an S_{VV} not necessarily highly correlated and equal in magnitude, Eq. (2) still indicates that σ^o_{RL} will be small and σ^o_{RR} will be large when the polarimetric phase difference is close to 180°. In the three test sites that we studied, large values of σ^o_{RR} usually resulted in an overestimation of forest biomass. This was typically the case of flooded forest, wet or damaged trees, and sparse and tall forest, where trunk-ground scattering is often a strong contributor to total radar backscatter. Clearly, these restrictions on the type of forest that could be monitored at circular polarization are very strong, and we may conclude that the use of circular polarization for monitoring forest biomass from space is of limited value

4. Biomass mapping in tropical rain forests

Figure 1a shows a false color composite image of the lower Rio Manu and Rio Pinquina in Peru acquired at P-band on June 7, 1993 by the NASA/JPL AIRSAR instrument. In this color representation, red corresponds to double-bounce scattering, green to diffuse scattering and blue to single-bounce scattering. The intensity of each color is proportional to the contribution of each one of the above-mentioned simple form of scattering to total radar backscatter. This image is obtained from a Cloude decomposition of the polarimetric signature of the imaged surface using the algorithm described in [3]. This mathematical decomposition of the scattering matrix provides a description of the type of interaction of the radar signals with the forest canopy and facilitates data analysis. Most major vegetation types (Fig. 2) are separated in this scattering mechanism map. Palm forests with an open canopy appear red at the center left of the scene, indicating a scattering dominance from double-bounce interactions. Tall floodplain forests (center and upper part) appear yellow, a combination of double-bounce scattering and volume scattering. Surrounding them, large and dense mosaic forest canopies appear green or red-dotted, indicating scattering dominance from the branches and occasionally double bounce reflections. Adjacent to the river, early successional stages of short *Tessaria* forests appear green-brown, thereby dominated by branch volume scattering but with weak radar echoes, consistent with their low biomass. Taller *Gynerium* forests in dark green and a zone of *Cecropia* forest in lighter green are further away from the river. Transition to taller mosaic forests, characterized by *Ficus insipida* (Moraceae) and *Cedrela odorata (Meliaceae)*, appear light green-red dotted. There, the zonation of the previous phases is diminishing and the color separation is more diffuse. In the top portion of the scene, the upland and hill forests between the Rio Manu and the Andes appear to have a higher component of tall deciduous trees (colored green-yellow) than the floodplain forests (colored green) between the lower Rio Manu and the hill area at the bottom of the scene. This effect may however be caused by differences in incidence angle of the radar illumination changing from about 30 to 55°. In the hill area to the bottom of the scene, regular hills of 30-50 m elevation yield a pronounced textural modulation of the SAR signal.

In contrast, the L- and C-band Cloude decompositions (Fig. 1b and 1c) show much less separability in scattering behavior between major vegetation types. This result may be attributed to the larger penetration of P-band signals which are able to interact with subcanopy structures. The higher frequency signals are limited to interactions in the upper canopy of the forests, where distinctions between major vegetation types are less apparent. The blue tone of the C-band decomposition illustrates that C-band radar returns contain a mixture of volume scattering from the upper branches and single bounce reflections from the top of the canopy. As the frequency is reduced, the color tone of the forest becomes more yellow, indicating an increasing significance of trunk-ground scattering.

The vegetation types of the Manu area (Fig. 2) contain a wide range of forest volume. We developed an empirical relationship between forest biomass and radar backscatter for this area to generate a map of forest biomass. At the low biomass levels (< 10 kg/m^2), we used the regression curve which was developed for Alaskan forests and which utilized the P-band HH-, HV-, and VV-polarized data gathered during the dry season (Table 1). At the higher biomass levels, the regression curve correctly separated the different classes of biomass, but underestimated forest biomass quite significantly. We modified the regression to increase the predicted biomass levels for large radar backscatter values and obtain a better agreement with our ground estimates.

Areas where the forest biomass predicted from the radar exceeds 30 kg/m^2 (dark green) correspond to the mature floodplain forests (colored yellow in Fig. 1a), and where woody biomass is indeed expected to be the largest (Fig. 2). The forest floor in the imaged broadleaf forests was dry at the time of the AIRSAR overflight (the dry season ends in September), so the enhanced radar signature of these stands at HH-polarization is not caused by wetter ground layers but more likely by tall tree trunks of large diameter. Forest biomass is lower in palm forests (green), which are surrounded by broadleaf forests of higher biomass (dark green). Old meanders, sealed off by freshly deposited sediment and showing as oxbow lakes (Cochas) with open water are mapped as areas of no biomass (black). Low biomass (brown) is estimated along the termini of Cochas, having an early succession of sedges, grasses and sill'III)s (especially *Annona tessmannii* (Annonaceae)), which are occasionally intercut by a tall stand of *Heliconia episcopalis* (Musaceae) with slightly larger biomass (oxbow at center right of the scene, green). In the expanding meander loop, in the center left of the image, that points down towards the lower border of the river, the early succession of riparian vegetation is well discriminated in the biomass map. Forest succession starts from the beach with short, even-aged stands of fast-growing *Tessaria* shrubs, followed by *Gynerium* stands (6 m in height) with higher biomass (dark brown). Adjacent are older successional stages of *Tessaria-Gynerium* (10-12 m in height) (light brown), and pure *Gynerium* (yellow). Continuing inland, towards the top of the scene, are deciduous leafless trees species mixed with *Cecropia* (10 26 m) above a 5 m-tall understory of *Gynerium*. This forest appears blue green in Fig. 1d, and corresponds to a higher biomass level. A mosaic of semi-deciduous floodplain forest (30-35 m) with higher predicted biomass follows. This type of clearly zoned and highly productive riparian forest succession, where each stage reaches a greater absolute height than the previous one, is characteristic of this area and can be identified at many locations along the river in Fig. 1(1. For instance, to the right of the previous meander, *Gynerium* and scattered *Tessaria* (10-12 m) on the upper bank, and *Gynerium* (5 m) with scattered leafless trees (25 m) on the lower bank are ('0101 ('(1" lightbrown and yellow as they indeed correspond to intermediate ranges of low biomass of about 4 kg/m^2. The extensive stands of *Cecropia* forest next to these correctly appear as areas of intermediate biomass (yellow).

In the hill-areas at the bottom of Fig. 1(1, the spatial variability in radar backscatter is controlled by surface topography and forest biomass is not correctly represented. There, a digital elevation model of the terrain is needed to correct the data from topography-induced calibration errors, and to retrieve forest biomass as a function of the incidence angle.

5. Conclusions

A comparison of radar-derived estimates of forest biomass with estimates obtained from forest inventory and allometric equations in three test sites of temperate and boreal forests shows that the average absolute error in predicted biomass is about 10 to 30 % of the actual biomass, depending on the complexity of the forest. These error rates, obtained using linearly polarized signals, increase significantly when circular-polarized signals are used. Combining HH-, HV-, and VV-polarizations also provides better estimates of forest biomass than using HV-polarization alone. The inversion technique used here is relatively straightforward. It is based on a linear regression that ignores structural differences between tree species and is optimized for forested areas image at about 45° incidence angle. There are also large uncertainties associated with ground measurements of forest biomass in natural ecosystems. It is expected that these estimates could be improved significantly by including incidence angle effects, dependence on tree species, inundation and soil property information, and surface topography. In tropical forests, the example of the Manu forest illustrates that longer wavelength imaging radars can become very useful for mapping forest types in tropical areas, where substantial below-canopy biomass differences cannot be derived from the top forest canopy properties, and remote sensors operating at optical wavelengths are impeded by a persistent cloud cover. Imaging radars also perform better than expected as tools for estimating woody biomass in tropical forests. The worldwide need for large scale, updated biomass estimates, achieved with a uniformly applied method, justifies a more in-depth exploration of long wavelength imaging radar applications for tropical forests inventories.

Acknowledgements The authors would like to thank John Terborgh, Sharon Billings, Bruce Chapman and Viviana Horna -Rodriguez for help in getting the ground truth data in Peru; Thuy Le Toan for providing the ground truth data for the Landes forest; Eric Kasischke for providing the ground truth data for the Duke University Forest; and Jeff Klein for comments on the manuscript. This work was carried out at the Jet Propulsion Laboratory, California Institute of Technology, under contract with the National Aeronautics and Space Administration.

References

[1] Le Toan T., A. Beaudoin, J. Riom and 1). Guyon, Relating forest biomass to SAR data, *IEEE Trans. on Geosc. and /<(7)1. Sens.* 30, 403 411, 1992.

[2] Kasischke E.S., L.L. Bourgeau-Chavez, N.L. Christensen and M.C. Dobson, The relationship between above- ground biomass and radar backscatter as observed 011 airborne SAR imagery, *Proc. of the Third AIRSAR Workshop* (Pasadena, CA), May 23-24, 1991, (.11'1, Pub. 91-30) pp. 1121, 1991.

[3] Dobson M.C., F.T. Ulaby, 'J'. LeToan, A. Beaudoin, E. S. Kasischke and N. Christensen, Dependence of radar backscatter on conifer forest biomass, *IEEE Trans. on Geosc. and Rem. Sens.* 30, 412-415, 1992.

[4] Rignot E., C. Williams, J.B. Way, and L. Viereck, Radar Estimates of Above-ground Biomass in Boreal Forests of Interior Alaska, *IEEE Trans. on Geosc. and Rem. Sens.*, 32, 1117-11241, 1994.

[5] Beaudoin A., T. Le Toan, S. Goze, E. Nezry, A. Lopes, E. Mougin, C.C. Hsu, H.C. Han, J.A. Kong and 1{,' 1'. Shin, Retrieval of forest biomass from SAR data, *Int. J. of Rem. Sens.*, In Press.

[6] Hsu C.C., H.C. Han, R.T. Shin, J.A. Kong, A. Beaudoin and '1', Le Toan, Radiative transfer theory for polarimetric remote sensing of pine forest, *Int. J. of Rem. Sens.*, In Press.

[7] van Zyl J .,1., The effect of topography on radar scattering from vegetated areas, *IEEE Trans. on Geosc. and Rem. Sens.* 31, 1 53- 160, 1993.

[8] Lang, I{.II,, N.S. Chauhan, K.J. Ranson and (). Kilic, Modeling P-band SAR returns from a red pine stand, *Rem. Sens. Environ.* 47, pp. 132-1 1 I , 1994.

[9] Ogawa, I I., K. Yoda, K. Ogina and '1'. Kira, Comparative ecological studies on three main types of forest vegetation in Thailand II. Plant biomass, *Nature and life in* ,S,1,'. *Asia* 4, pp. 4()- 80, 1 965.

[10] Huttel, C., Root distribution and Biomass in three ivory coast rain forest plots, in *Tropical ecological systems. Ecological studies* Medina E. and ('olly F. (eds .), Vol. 11. Springer Verlag , New York, pp. 123 130, 1975.

[11] Fearnside, P. M., L. Niwton and F. M. Fernandes, Rainforest burning and the global carbon budget: biomass, combustion efficiency, and charcoal formation in the Brazilian Amazon, *J. Geophys. Res.*, 98, pp. 16733-16743, 1993.

[12] Whittaker, R.H. and G.E. Likens, Carbon in the biota, in *Woodwell GM and Pecan EV (eds) Carbon and the Biosphere*, Nat Tech. Infor. Center, Springfield, Va., pp. 281:100," 1973.

[13] Rodin, L.E., N.I. Bazilevich and N.N. Rozov, *Productivity of the World main ecosystems*, Reichle D.E., Franklin J.F., Goodall (((is.), National Academy of Sciences, Washington D. C., 1975.

[14] Lieth, H. Primary productivity in ecosystems: Comparative analysis of global patterns, in *Unifying concepts in Ecology* p. 67-88. Rep. Plen. Sess. First Intern. Congr Ecol. The Hague, The Netherlands 1974. van Dobben W.H., Lowe-McConnell R.H. (((IS.), The Hague, W. Junk Publishers, 302 pp., 1975.

[15] Botkin, D.B. and L.G. Simpson, Biomass of the North American boreal forest : a step forward toward accurate global measures, *Biochemistry*, 9, pp. 161- 174, 1990.

[16] Botkin, D.B., L.G. Simpson and R. A. Nisbet, Biomass and carbon storage of the North American deciduous forest, *Biochemistry*, 20, pp. 1- 17, 1 993.

[17] I)\'tills, J,V. and T. Hagfors, Radar astronomy, McGraw- Hill, Inc., New York, 620 p., 1968.

[18] Freeman, A., J. Cruz, B. Chapman, M. Alves. J. Sun. M. Azeem and S. Shaffer, First results from SIR-C calibration, in *Proc. Int. Geosc. Rem. Sens. Symp. IGARSS'94*, Pasadena, California, August 8-12, Volume 11, IEEE Catalog 94CH3378-7, pp. 1079 1081, 1994.

[19] Bolin, B., '1'. Degens, S. Kempe and P. Ketner, *'I'lIt global carbon cycle* Scope 13, John Wiley and Sons, Chichester, 1979.

[20] Art H.W. and Marks 1'.1,., A summary table of biomass and net annual primary production in forest ecosystems of the World, in *Forest biomass studies*, Sec. 25, p. 3-32, Growth and yield, 15th. Internat Union Forest Res. Organ. Congr. 1971 , 205 pp., 1971.

[21] Terborgh, J., *Five New World Primates: A study in* (.'()?//])(I? '(///'(*Ecology*, Princeton University Press, Princeton, NJ, 1983.

[22] Terborgh, J., Habitat selection in Amazonian birds, in *Habitat Selection in Birds* (Ed. M.L. Cody), Academic Press, New York, pp. 311-318, 1985.

[23] Kalliola R., Salo J. and Mäkinen Y., Regeneracion natural de selvas en la Amazonia Peruana 1: dinamica fluvial y sucesion riberena. *Memorias del Museo de historia Natural 'Javier Prado'* (Lima), 18, pp. 1-102, 1987.
[24] Sanchez, W.G., Aspectos taxonómicos, fitosociologicos y aplicados del género ceropia en el Valle de Kcosñipata y el Manu, Thesis, Universdad Nacional de San Antonio Abad del Cusco, Peru 1976.
[25] FAO-UNESCO-UNEP, *Tropical forest ecosystems*, Chap. 10, Gross and net primary production and growth parameters, pp. 233-248, 1978.
[26] Walter, H., Breckle S.W., *Ecological systems of the Geobiosphere, Tropical and subtropical zonobiomes*, Vol. 2, Springer Verlag, Berlin, 465 pp., 1984.
[27] Tosi, J.A., Zonas de vida natural en El Peru, Instituto Interamericano de Ciencias Agricolas de la OEA Zona Andina, *Boletin Tecnico* 5, 271 pp., 1960.
[28] Walter, H. and S.W. Breckle, *Ecological systems of the Geobiosphere, Temperate and polar biomes other than northern Eurasia*, Vol. 4, Springer Verlag, Berlin, 1991.
[29] FAO, *Forest resources assessment 1990, Tropical countries*. FAO Forestry Paper, 112, Rome, 1993.
[30] Nghiem, S.V., S.H. Yueh, R. Kwok, and F.K. Li, Symmetry properties in polarimetric remote sensing, *Radio Sci.*, **27**, pp. 693-712, 1992.
[31] van Zyl, J.J., Application of Cloude's target decomposition theorem to polarimetric imaging radar data, *Proc. SPIE*, Vol. 1748 Radar Polarimetry, pp. 184-191, 1992.

Table 1 Error rates of predicted biomass from the radar at different polarizations for three different forest sites. The regression curve for the calibrated data acquired over BCEF on July 21, 1993 is: $Log(B) = 4.7610 + 0.3585\,\sigma^o_{HV} + 0.00613\,\sigma^{o2}_{HV} - 0.4467\,\sigma^o_{HH} - 0.0269\,\sigma^{o2}_{HH} - 0.0292\,\sigma^o_{VV} - 0.0053\,\sigma^{o2}_{VV}$, where B is expressed in kg $/m^2$ and the radar backscatter values σ^o are expressed in dB. Lin.Pol. means linear polarization. Cir.Pol. means circular polarization. R^2 is the R-squared coefficient of the regression, indicated in parenthesis

Forest Site (Date Acq.)	Combination	Error Linear Pol. % (R^2)	Error Circular Pol. % (R^2)	Polarization
Landes, FR	HH, HV, VV	12 (0.99)	11 (0.99)	RL, RR
(08-16-89)	HV	13 (0.99)	12 (0.99)	RR
Duke, NC	HH, HV, VV	29 (0.92)	36 (0.89)	RL, RR
(09-02-89)	HV	33 (0.90)	46 (0.83)	RR
BCEF, AK	HH, HV, VV	28 (0.95)	107 (0.87)	RL, RR
(05-03-91)	HV	45 (0.85)	131 (0.78)	RR
BCEF, AK	HH, HV, VV	21 (0.97)	52 (0.88)	RL, RR
(05-06-91)	HV	29 (0.90)	109 (0.79)	RR
BCEF, AK	HH, HV, VV	19 (0.99)	27 (0.97)	RL, RR
(07-21-93)	HV	31 (0.91)	38 (0.94)	RR

Figure 1. False color composites of a 10 km x 10 km radar image of the Manu National Park Forest, in south-eastern Peru. AIRSAR is flying from left to right, illuminating the surface from the top. Spatial resolution is about 15 m on the ground. (a), (b) and (c) are the results of a Cloude decomposition of polarimetric scattering at (a) P-band, (b) L-band and (c) C-band. Single-bounce scattering is colored blue, double-bounce scattering is colored red, and diffuse scattering is colored green. Color brightness is proportional to the intensity of the radar echoes in each one of the three canonic scattering modes. The Rio Manu (flowing from left to right) and Rio Pinquina (entering Rio Manu from the top) appear as dark features. (d) is a map of forest biomass between 0 and greater than 30 kg/m^2 for that same area and obtained using a multilinear regression between radar backscatter and forest biomass.

Figure 2. Major vegetation types of the Rio Manu Area. Forest succession on alluvial floodplains is initiated by disturbance due to flooding in the rain season (October to March). Rapid growing stands of *Gynerium* and *Tessaria* are eventually replaced by *Cecropia*. Abandoned high river beds may turn into palm dominated areas (Aguajales) with seasonally varying degree of standing waters. On undisturbed areas, a mosaic forest develops which will eventually become a mature floodplain forest after a 100 to 200 years. On adjacent hills, the forest is undisturbed, but lower nutrient availability and temporal soil drought cause the development of a shorter forest with seasonal deciduousness. (Drawings: R. Zimmermann)

CLOUDE DECOMPOSITION MANU NL PARK, PERU (3700)

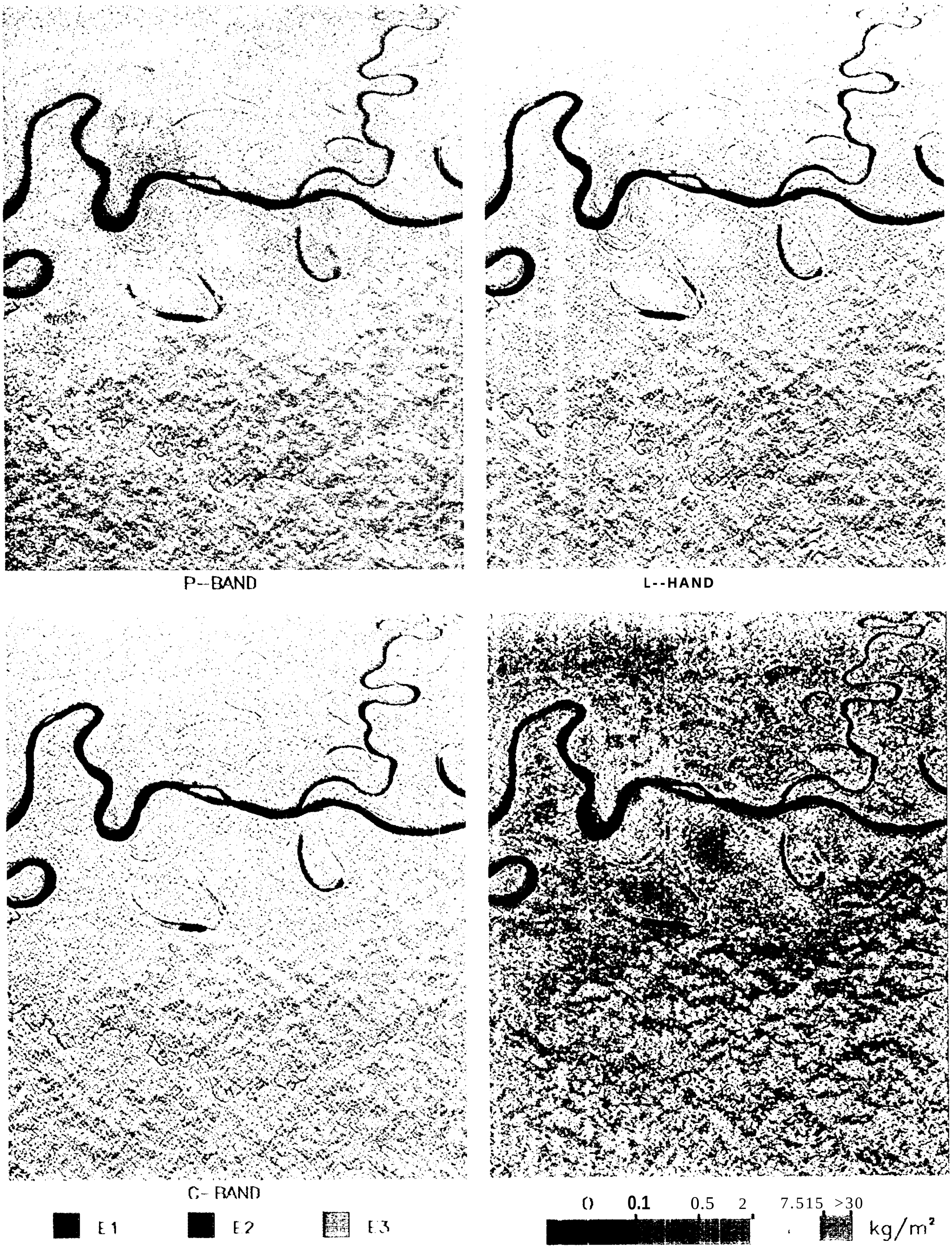

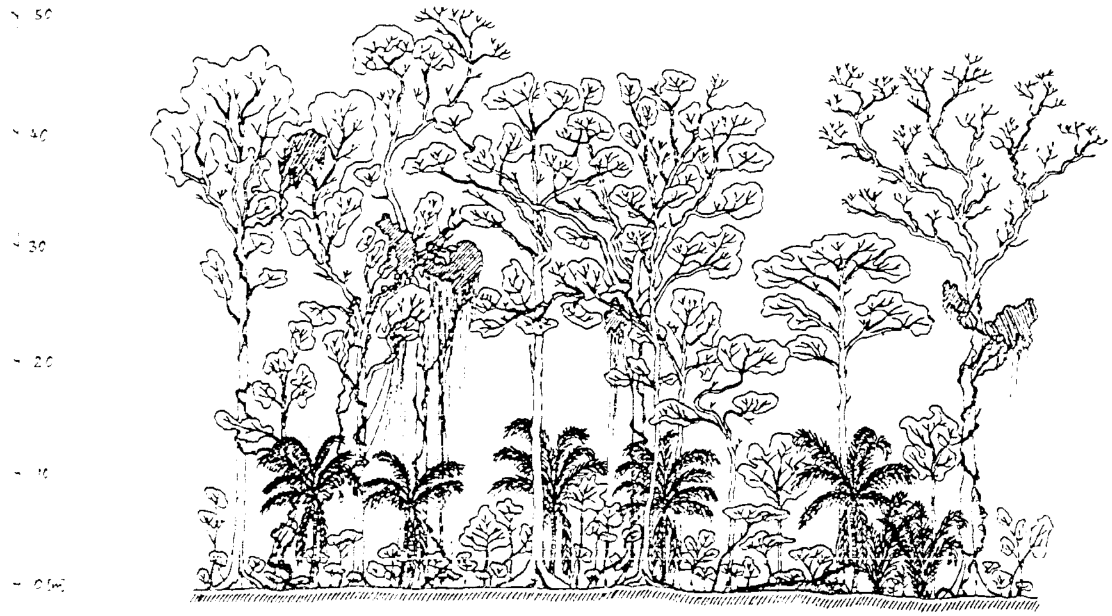

Mature Floodplain forest

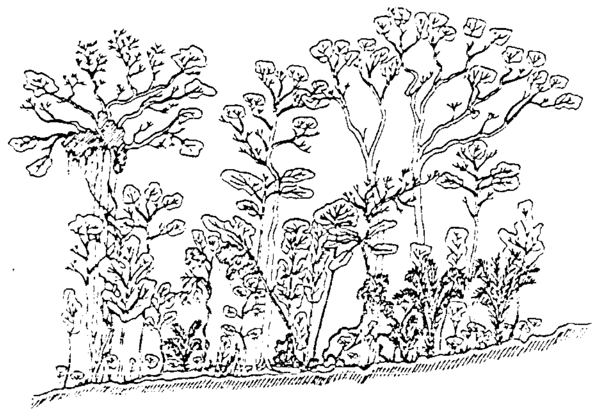

Mature Upland Forest

Disturbed Mosaic forest

Palm Aguajal

Cecropia stand
with *Gynerium* understory

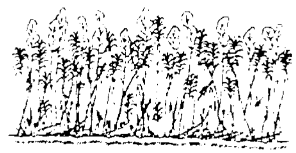

Mature *Tessaria* stand
with *Gynerium* understory

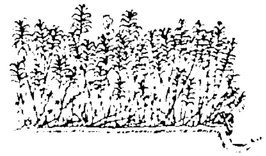

Gynerium stand